frontiers | Frontiers in Nutrition

ORIGINAL RESEARCH
published: 24 May 2022
doi: 10.3389/fnut.2022.887064

The Effect of Glycosylated Soy Protein Isolate on the Stability of Lutein and Their Interaction Characteristics

Xia Wang[1], Shaojia Wang[1], Duoxia Xu[1], Jingwei Peng[2], Wei Gao[2]* and Yanping Cao[1]**

[1] Beijing Advanced Innovation Center for Food Nutrition and Human Health (BTBU), School of Food and Health, Beijing Higher Institution Engineering Research Center of Food Additives and Ingredients, Beijing Technology and Business University (BTBU), Beijing, China, [2] Chenguang Biotech Group Co., Ltd., Handan, China

OPEN ACCESS

Edited by:
Biao Yuan,
China Pharmaceutical University, China

Reviewed by:
Qian Zha,
Shanghai Academy of Agricultural Sciences, China
Zufei Xiao,
Bavarian Office for Forest Seeding and Planting, Germany

***Correspondence:**
Shaojia Wang
wangshaojia@btbu.edu.cn
Wei Gao
gw@cn-cg.com
Yanping Cao
caoyp@th.btbu.edu.cn

Specialty section:
This article was submitted to Food Chemistry, a section of the journal Frontiers in Nutrition

Received: 01 March 2022
Accepted: 11 April 2022
Published: 24 May 2022

Citation:
Wang X, Wang S, Xu D, Peng J, Gao W and Cao Y (2022) The Effect of Glycosylated Soy Protein Isolate on the Stability of Lutein and Their Interaction Characteristics. Front. Nutr. 9:887064. doi: 10.3389/fnut.2022.887064

Lutein is a natural fat-soluble carotenoid with various physiological functions. However, its poor water solubility and stability restrict its application in functional foods. The present study sought to analyze the stability and interaction mechanism of the complex glycosylated soy protein isolate (SPI) prepared using SPI and inulin-type fructans and lutein. The results showed that glycosylation reduced the fluorescence intensity and surface hydrophobicity of SPI but improved the emulsification process and solubility. Fluorescence intensity and ultraviolet–visible (UV–Vis) absorption spectroscopy results showed that the fluorescence quenching of the glycosylated soybean protein isolate by lutein was static. Through thermodynamic parameter analysis, it was found that lutein and glycosylated SPI were bound spontaneously through hydrophobic interaction, and the binding stoichiometry was 1:1. The X-ray diffraction analysis results showed that lutein existed in the glycosylated soybean protein isolate in an amorphous form. The Fourier transform infrared spectroscopy analysis results revealed that lutein had no effect on the secondary structure of glycosylated soy protein isolate. Meanwhile, the combination of lutein and glycosylated SPI improved the water solubility of lutein and the stability of light and heat.

Keywords: soy protein isolate, inulin-type fructans, lutein, stability, interaction

INTRODUCTION

Lutein, an oxygen-containing fat-soluble carotenoid, is widely distributed in flowers, vegetables (1), fruits, egg yolks (2), algae, grains (3), etc. and is mainly derived from marigolds (4). Lutein is also present in the macular pigment of human eyes and plays an indispensable role in preventing eye diseases, such as age-related macular degeneration (AMD) (5). However, it cannot be synthesized within the human body and should be supplied from external sources, such as food (6). Lutein possesses a carbon skeleton and a polyolefin chain (7), a major chromophore group (8). The carbon chain is supported by hydroxyl-containing ionone rings on each side with three stereocenters, β-ionone ring containing a stereo center (3R), and ε-ionone ring containing two stereocenters (3′R and 6′R) (9). The eight conjugated olefins in the carbon chain of the lutein molecule make lutein susceptible to degradation by the external environment (10).

The encapsulation systems, including liposomes, emulsions, gels, and molecular complexes, are often used to inhibit the degradation and improve the stability of biologically active substances, such as lutein (11). Of them, the macromolecules' cavity (such as protein) has attracted increasing interest in the encapsulation of biologically active substances. It is reported that egg white albumin improves the stability of marigold lutein ester extract during storage, and lutein dipalmitate binds spontaneously to egg protein through van der Waals forces and hydrogen bonding (12). Yi et al. (13) found that the stability of lutein increased with the increase of milk protein content, the protective effect of sodium caseinate (SC) on lutein was stronger than the whey protein isolate (WPI), and the milk protein interacted with lutein through hydrophobic bond.

Soy protein isolate (SPI) is a plant protein (about 90% protein) with high nutritional value and is widely used in the food industry (14, 15). It is mainly composed of β-conglycinin (7S, 180–210 kDa) and glycinin (11S, approximately 360 kDa) and accounts for about 70% of the total protein. The 11S component consists of 6 acidic and 6 basic polypeptide chains linked together by disulfide bonds, whereas the 7S is stabilized by hydrophobic interactions (16). In recent years, SPI has been used as a carrier in food-grade delivery systems to improve the stability of biologically active substances. Cao et al. (17) found that SPI could improve the thermal stability of chlorophyll. Tapal and Tiku (18) improved water solubility and bioavailability of curcumin using SPI. Wan et al. (19) also showed that SPI could be used as a carrier of resveratrol (RES) in functional foods, which could improve the water solubility and stability of RES. However, the functional properties of SPI, such as solubility in neutral and mildly acidic environments, severely limit its use as an encapsulation wall material. As such, the physical, chemical, and enzymatic properties of SPI are often modified (16). Physical modification mainly relies on high temperature and high pressure or shearing, making the equipment requirements relatively high and large-scale production difficult. Enzymatic modification is expensive, and protein hydrolysis can make the taste worse. Chemical modification has a high effect on the functional properties of the protein, mainly by introducing food-grade ingredients (20). Glycosylation is a typical chemical modification, which modifies the structure of the protein and improves the functional properties of the protein through a covalent bond between the amino groups of protein and the carbonyl group of the reducing sugar (21). The glycosylation of glucan and protein improves the freeze–thaw stability of SPI hydrolysate (SPIH) emulsion (22), the binding and transporting ability of casein phosphopeptide to calcium (23), the solubility, emulsifying, and foaming ability of peanut protein isolate (24). The emulsifying properties and emulsifying stability of the conjugates of inulin and WPI were significantly higher than the WPI at a pH of 3–7 (25). Inulin-type fructans (ITFs) are linear fructose polymers with predominantly or only β-(2→ 1) fructosyl–fructose linkages (26). Stabilizing the intestinal mucosal barrier, reducing the risk of colon cancer, promoting calcium absorption, and improving constipation are the physiological functions of ITFs (27–33). ITFs are widely used as a prebiotic food ingredient (34). However, the modification effects of ITFs on SPI and ITF-modified SPI on the stability of lutein are still unknown.

Therefore, the present study aimed to study the modification effect of ITFs on SPI and ITF-modified SPI (glycosylated soybean protein isolate, GSPI) on the stability of lutein and the interaction between GSPI and lutein. The study results will provide insights into the preparation of protein-encapsulating systems for embedding lutein and other similar biologically active compounds.

MATERIALS AND METHODS

Materials

Soy protein isolate was purchased from Shanghai Yuanye Bio-Technology Co., Ltd. (Shanghai, China). ITFs and lutein extract were provided by Chenguang Biotech Group Co., Ltd. (Hebei, China). Phosphates were purchased from Shanghai Aladdin Biochemical Technology Co., Ltd. (Shanghai, China). Lutein (97%) was purchased from ChromaDex, USA. Bovine serum albumin (BSA, purity 97%) was obtained from Beijing Solarbio Science and Technology Co., Ltd. (Beijing, China). Sodium 8-naphthalenesulfonate-1-anilino (ANS) ≥97% was purchased from Shanghai Macklin Biochemical Technology Co., Ltd. (Shanghai, China). G250 Coomassie Brilliant Blue Ultra pure grade was purchased from Beijing Boao Tuoda Science and Technology Co., Ltd.

Absolute ethanol (chromatographic grade), methyl tert-butyl ether (chromatographic grade), methanol (chromatographic grade), cyclohexane (chromatographic grade), and N-hexane (chromatographic grade) were purchased from Beijing Merida Technology Co., Ltd. (Beijing, China). Ethyl acetate (analytical grade) and potassium hydroxide (KOH) (analytical grade) were purchased from Tianjin Fuchen Chemical Reagent Company (Tianjin, China). 2, 6-Di-tert-butyl-*p*-cresol (BHT) (analytical grade) was purchased from Shanghai Macklin Biochemical Technology Co., Ltd. (Shanghai, China).

Sample Preparation

Soy protein isolate and ITFs (mass ratio 1:1) were stirred overnight with 10 mM Na_2HPO_4 to make them fully hydrated and adjusted to pH 11 with 0.1 M NaOH to make the final protein concentration of 2% (w/v). The SPI/ITF mixtures were incubated in a water bath at 100°C for 4.7 h (previous research work has confirmed that the GSPI has the highest emulsification ability under this experimental condition). HSPI was the only heated SPI (100°C for 4.7 h), and G-SPI was the physical mixture of SPI and ITFs.

Lutein extract was dissolved in absolute ethanol and stored at 4°C protecting from light. The lutein content in the lutein ethanol solution was expressed as 10 mg/ml with 97% lutein standard product.

For stable analysis of protein and lutein complexes preparation, 15 ml of GSPI and SPI were adjusted to pH 7.0, and then 0.5 ml of lutein extract in absolute ethanol was added dropwise to GSPI and SPI, respectively. Finally, the volume was adjusted to 100 ml with 10 mM pH 7.0 phosphate-buffered saline (PBS) and incubated for 1 h at room temperature.

The complexes of different concentrations of 97% lutein (10, 20, 30, 40, 50, 60, and 70 μM) and GSPI (0.2 mg/ml) were also prepared to explore the interaction between lutein and protein.

Fourier Transform Infrared Spectroscopy

The freeze-dried sample was mixed with KBr at a ratio of 1:100 with KBr as the background. The wave number was 400–4,000 cm^{-1}, and the resolution was 4 cm^{-1} for 32 scans with IS5 infrared spectrometer (Thermo Fisher, USA).

The spectral range of 1,700–1,600 cm^{-1} (amide I) of GSPI and GSPI–lutein were subjected to Fourier deconvolution and second derivative analysis by PeakFit 4.12.

Fluorescence Spectrum

Later, 200 μl of all the samples were transferred to 96-well plates for fluorescence spectroscopy, and the intrinsic fluorescence spectrum was measured by M200 Pro TECAN Infinite multifunctional microplate reader (Tecan Inc., Switzerland).

Excitation Spectrum

The fluorescence excitation spectra of SPI, HSPI, G-SPI, and GSPI were measured at 293 K. The excitation wavelength was set from 250 to 380 nm and the emission wavelength was 420 nm (25).

Emission Spectrum

The fluorescence emission spectra of SPI, HSPI, G-SPI, and GSPI were measured at 293 K, and the fluorescence emission spectra of GSPI (0.2 mg/ml) and lutein (10, 20, 30, 40, 50, 60, and 70 μM) were measured at 293, 303, and 313 K. The emission wavelength was set from 310 to 460 nm, and the excitation wavelength was set at 280 nm, according to the method of Qi et al. (35).

The fluorescence quenching mechanism between GSPI and lutein was explored by the Stern–Volmer equation (1) (17):

$$\frac{F_0}{F} = 1 + K_{SV} \times [Q] = 1 + K_q \times \tau_0 \times [Q] \quad (1)$$

where, F_0 and F are the fluorescence intensity in the absence and presence of lutein. K_{SV} is the Stern–Volmer quenching constant. K_q is the bimolecular quenching rate constant. τ_0 is the average lifetime of the unquenched fluorophore, which is 10^{-8} s. [Q] is the concentration of lutein.

The double logarithmic Stern–Volmer equation was used to analyze the binding sites and binding constants of GSPI and lutein [Equation (2)]. The thermodynamic parameters of GSPI and lutein were determined by Equations (3, 4).

$$\log \frac{(F_0 - F)}{F} = log\, K_a + n\, log[Q] \quad (2)$$

where, n is the number of binding sites. K_a is the binding constant.

$$Ln\, K_a = -\frac{\Delta H}{RT} + \frac{\Delta S}{R} \quad (3)$$

$$\Delta G = \Delta H - T\Delta S = -RT\, Ln\, K_a \quad (4)$$

where, ΔH denotes the enthalpy change, ΔG denotes free energy change, and ΔS denotes entropy change. R denotes the gas constant 8.314 J/ (K mol). T (K) refers to different temperatures (20°C, 30°C, and 40°C).

Surface Hydrophobicity

The 1-anilino-8-naphthalenesulfonate (ANS) was used as a fluorescent probe to measure the surface hydrophobicity (H_0), according to the method of He et al. (20), with slight modifications. The sample was diluted with 10 mM pH 7.0 PBS to 0.01–0.09 mg/ml, then 2 ml of the protein sample was added with 40 μl ANS, and reacted for 10 min in the dark. Approximately 200 μl of each sample was transferred to a 96-well plate, and the fluorescence intensity was measured at 390 nm (excitation wavelength) and 470 nm (emission wavelength) using M200 Pro TECAN Infinite multifunctional microplate reader. The slope of the protein concentration and its corresponding fluorescence intensity were H_0.

Solubility and Emulsification

Solubility

The samples were centrifuged at 4,500 r/min for 15 min using an Avanti JXN-30 floor-standing centrifuge (Beckman, USA). The supernatant was diluted by 200 times, then 1 ml of the diluted solution was added with 5 ml of G250 Coomassie Brilliant Blue, mixed uniformly, and the absorbance was measured at 595 nm using an UVmini-1240 UV Spectrophotometer (Shimadzu, Japan). The samples were measured within 2–30 min. BSA was used as the standard curve to calculate the protein content.

Emulsification

Approximately 40 ml of GSPI and 10 ml of soybean oil were put into a 100-ml beaker, homogenized at a speed of 12,000 r/min for 2 min using T25 digital homogenizing and dispersing instrument (IKA, Germany) (36). Then, 50 μl was taken from the bottom and mixed with 5 ml of 0.1% SDS, and the absorbance values were measured at 500 nm. Afterward, 50 μl of deionized water and 5 ml of 0.1% SDS were adjusted to zero. The emulsifying activity index (EAI) was calculated by Equation (5).

$$EAI\ (m^2/g) = \frac{2 \cdot 2.303 \cdot A \cdot n}{C \cdot \left(1 - \text{“}\varphi''\right) \cdot 10^4} \quad (5)$$

where, A is the absorbance value at 500 nm, n is the dilution factor, C is the protein concentration (g/ml), and ϕ is the oil phase volume.

UV–Vis Absorption Spectroscopy

The mixtures of GSPI and lutein in 2.2 were diluted four times, namely GSPI (0.025 mg/ml) with lutein standards (2.5, 5.0, 7.5, 10, and 12.5 μM). The ultraviolet–visible (UV–Vis) spectra were measured in the wavelength range of 190–350 nm using a 10-mm quartz cell with TU-1900 Dual-Beam UV–Visible Spectrophotometer (Beijing Puxi General Instrument Co., Ltd., China.).

X-Ray Diffraction

The crystal of lutein, GSPI, and GSPI–utein was measured by a D8 Advance X-ray Diffractometer (Bruker Technology Co., Ltd., Germany) at a speed of approximately 2°/min and scanning at an angle (2θ) from 5° to 40°.

Stability of Lutein

Thermal stability: Around 8 ml of lutein, SPI–lutein, and GSPI–lutein were added into a pressure test tube, tightened the tube mouth, and then heated in an oil bath at 120°C for 50 min. The samples were taken every 10 min.

Light stability: Lutein, SPI–lutein, and GSPI–lutein were placed in a 100-ml sample bottle, irradiated under a 302-nm UV lamp for 12 h, and the samples were taken every 2 h for analysis. (The light was perpendicular to the sample, and the distance was about 2 cm.)

Color Measurements

The color characteristics were measured by a CR-800 Spectrophotometer under a reflection mode (Beijing Colorimeter Instrument Equipment Co., Ltd., China). The total color difference (ΔE) was calculated by Equation (6):

$$\Delta E = \sqrt{\left(L^* - L_0^*\right)^2 + \left(a^* - a_0^*\right)^2 + \left(b^* - b_0^*\right)^2} \quad (6)$$

where, ΔE means total color difference. L_0^*, a_0^*, and b_0^* mean the initial color values of the sample. L*, a*, and b* mean the color values of the sample at time *t*. L* means light and dark; a* means red and green, and b* means yellow and blue.

Content and Degradation Kinetics Analysis

Around 5 ml of the above sample was used for stability analysis. Then, 10 ml of absolute ethanol was mixed with 10 ml of 60% KOH, then shaken at room temperature for 3 h, and extracted with cyclohexane:*n*-hexane:ethyl acetate = 1:2:2. The extraction was repeated 3 times. The extracts were combined and rotary evaporated to near dryness in a 30°C water bath, then dissolved to 10 ml using a 0.1% BHT absolute ethanol for HPLC analysis. A standard curve was plotted using 97% lutein to characterize the content changes of lutein during the degradation process.

The change in lutein content was determined by Waters 2,695 HPLC (Waters Technology Co., Ltd., USA). The chromatographic column model was Venusil XBP C30 (5 μm, 250 mm × 4.6 mm). Phase A (methanol:water = 88:12), phase B (methyl tert-butyl ether). At 0–18 min, phase A changed from 100% to 10%; at 18.1 min, phase A changed from 10% to 100%, and kept it for 10 min. The flow rate was 1.0 ml/min, and the injection volume was 50 μl. The degradation rate was calculated by Equation (7), and the degradation kinetics was determined by Equations (8–10).

$$Degradation\ rate = \frac{C_0 - C_t}{C_0} 100\% \quad (7)$$

Kinetic equations (8–10) (37)

$$C_0 C_t = k_0 t \quad (8)$$

$$\mathrm{Ln}\left(C_t/C_0\right) = k_1 t \quad (9)$$

$$\frac{1}{C_t} - \frac{1}{C_0} = k_2 t \quad (10)$$

where, C_0 represents the initial content of lutein before stability analysis, and C_t represents lutein content at time *t* during stability analysis. k_0, k_1, and k_2 represent the kinetic constants.

Size Distribution

The particle size of lutein, GSPI, and GSPI–lutein was measured by an S3500 laser particle size analyzer (Microtrac, Germany). The sample was added dropwise to the sample cell until the screen showed ready, and then proceeded to the particle size distribution measurement.

Statistical Analysis

The images were generated by Origin 2021 software. The data were analyzed by one-way analysis of variance using IBM SPSS statistics 26. The significance analysis was done by LSD and Duncan's test ($p < 0.05$).

RESULTS AND DISCUSSION

Effect of Glycosylation on Protein Properties

Fourier Transform Infrared Spectroscopy

Fourier transform infrared (FTIR) could determine the occurrence of glycosylation reaction. The amide I bands (1,700–1,600 cm^{-1}) and amide II bands (1,600–1,500 cm^{-1}) of protein are the most sensitive regions related to protein conformation (38). The C=O stretching vibration of the peptide bond, the C–N stretching vibration of the amino group, and the N–H bending of the amino group are the characteristics of this amide zone (39). **Figure 1A** depicts the FTIR results of SPI, HSPI, ITFs, and GSPI under the range of 4,000–400 cm^{-1}. The amide I region of the GSPI absorption peak shifted from 1659.09 to 1658.38 cm^{-1}, and the absorption intensity was slightly reduced, which might be due to the decrease in the carbonyl content. The Schiff base and pyrazine formed during glycosylation showed an absorption at 1658.38 cm^{-1} (23). The amide II band shifted from 1536.99 to 1548.99 cm^{-1}, and the absorption peak of GSPI was stronger than SPI, indicating that the glycosylation product was formed by covalent bonds. This result was consistent with the results of glycosylated modified egg white protein pretreated by ball milling (40). The absorption intensity of GSPI was higher than SPI at the wavenumber of 1057.58 cm^{-1}, indicating that GSPI produces a new C–N covalent bond, which was consistent with the findings of WPI and inulin (25). Additionally, there was a

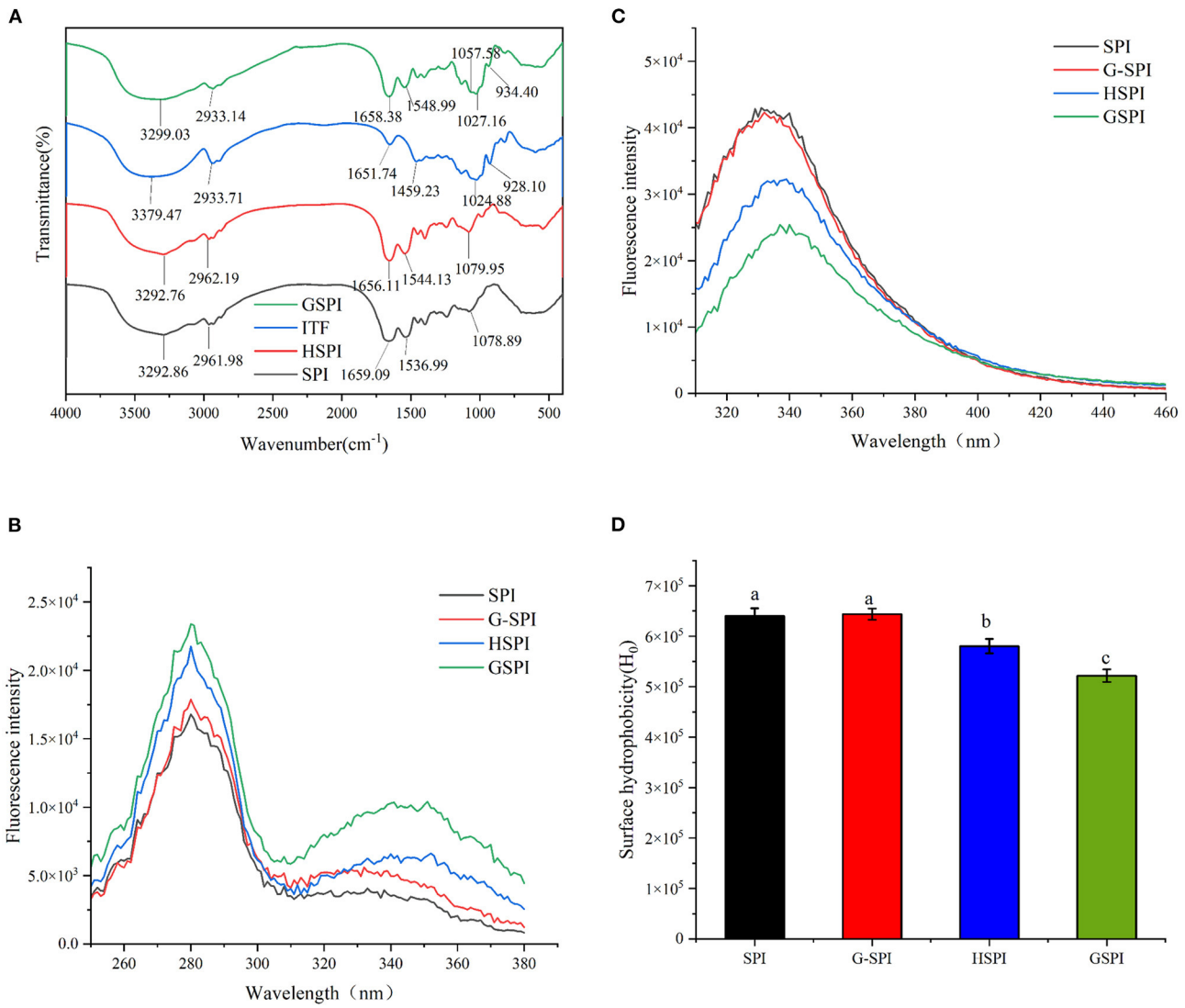

FIGURE 1 | (A) The Fourier transform infrared spectroscopy of SPI, HSPI, ITFs, and GSPI. **(B)** Fluorescence excitation spectroscopy of 0.1 mg/ml SPI, HSPI, G-SPI, GSPI, $T = 293$ K, pH = 7.0, $\lambda_{ex} = 280$ nm, and $\lambda_{em} = 310–460$ nm. **(C)** Fluorescence emission spectroscopy of 0.1 mg/ml SPI, HSPI, G-SPI, GSPI, $T = 293$ K, pH = 7.0, $\lambda_{em} = 420$ nm, and $\lambda_{ex} = 250–380$ nm. **(D)** Surface hydrophobicity of 0.01–0.09 mg/ml SPI, HSPI, G-SPI, GSPI, $T = 293$ K, pH = 7.0, $\lambda_{em} = 470$ nm, and $\lambda_{ex} = 390$ nm. Different letters indicate significant differences.

broad stretching vibration peak at 3,700–3,200 cm^{-1}, intimating the existence of hydrogen bonds and the increase of free hydroxyl content. This result was consistent with the Maillard reaction products of whey protein and flaxseed gum (41).

Fluorescence Intensity

Glycosylation is a chemical method for modifying proteins by covalent bonding between the proteins and sugars (40). The fluorescent substances with characteristic peaks between 340 and 370 nm are produced during a reaction (42). As depicted in **Figure 1B**, SPI, HSPI, G-SPI, and GSPI had a characteristic protein excitation wavelength at 280 nm, whereas GSPI had another maximum excitation wavelength at 351 nm. These results confirmed the occurrence of the Maillard reaction and the production of fluorescent substances. This was consistent with the previous research result showing that WPI and inulin had a maximum fluorescence excitation wavelength of 344 nm (25). **Figure 1C** depicts the fluorescence emission spectrum, indicating that the fluorescence intensity of SPI and G-SPI had not much difference. The fluorescence intensity of GSPI was less than SPI, suggesting that ITFs had a shielding effect on the fluorescence of SPI. Some previous studies had also manifested that the fluorescence intensity of glycosylated protein was less than the original protein (43), and this effect increased with the decrease of dextran molecular weight. Notably, heating increased the fluorescence intensity of the protein, and the fluorescence intensity of WPI increased by dry heat treatment (44). However, in this study, the fluorescence intensity of HSPI was less than

SPI. Therefore, it was speculated that this phenomenon was caused by extreme pH. Zhao et al. (45) revealed that extreme alkaline pH treatment of PSE-like chicken proteins had the same result.

Surface Hydrophobicity

Surface hydrophobicity is one of the essential functional properties of the protein, reflecting protein conformation and structure (46). ANS is commonly used as a probe to determine H_0 of proteins, which binds to the hydrophobicity of proteins efficiently (47). **Figure 1D** depicts the change in H_0 of SPI, G-SPI, HSPI, and GSPI, indicating that the physical mixture of SPI and ITFs was not significantly different from the H_0 of SPI. Compared with SPI, the H_0 of HSPI was significantly lower, which might be due to the fact that the alkaline conditions could make the protein fold and reduce the exposure of the SPI hydrophobic group. The H_0 decreased significantly after glycosylation and the exposed hydrophobic groups of SPI bound to ITFs, resulting in a decrease in H_0. In previous studies, the same results were obtained after glycosylation of SPI with *Pleurotus eryngii* polysaccharide (PEP) or dextran (DX) (20, 43). H_0 was consistent with the fluorescence emission spectroscopy results, and similar results were obtained under extremely acidic pH excursions and mild heating conditions for SPI (48).

Emulsification and Solubility

The EAI of protein is involved in several parameters, such as solubility, hydrophobicity, and structural flexibility (49). EAI is often used to indicate the emulsification of protein. As shown in **Figure 2A**, The EAI of SPI and GSPI were measured at different pH conditions, and the results showed that the emulsifying ability of GSPI was greater than SPI under the pH range of 5.5–7.5. Compared with GSPI, the EAI values of SPI were much more affected by pH. The poor solubility of SPI limits its application. The solubility of glycosylation significantly increased, and the protein content of GSPI diluted by centrifugation was 56.29 ± 0.96–59.30 ± 1.85 μg/ml, with no significant change in pH 5.5–7.5, whereas SPI had poor solubility in neutral and weakly acidic conditions (**Figure 2B**).

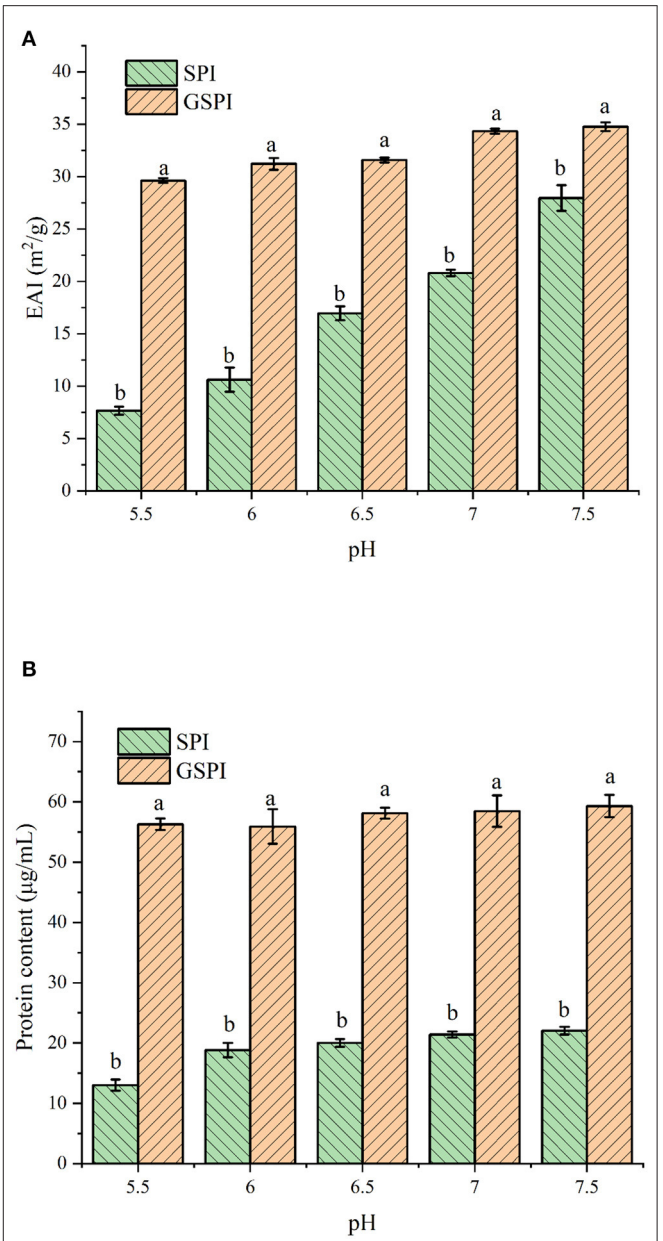

FIGURE 2 | (A) Emulsification of SPI and GSPI at pH 5.5–7.5. **(B)** Solubility of SPI and GSPI at pH 5.5–7.5. Different letters indicate significant differences between SPI and GSPI at the same pH.

Interaction Between GSPI and Lutein

Fluorescence Quenching

Fluorescence quenching methods could reveal the protein conformation and/or dynamic changes in the macromolecular systems. The Stern–Volmer equation is the easiest method to determine the quenching pattern (50). Quenching occurs when the quencher is located near or in contact with the fluorophore (51). Protein fluorescence arises from the presence of multiple fluorophores, mainly including three aromatic amino acids—Phe, Tyr, and Trp (52). The changes in the amino acid environment change the fluorescence intensity. As depicted in **Figure 3A**, with the increase of lutein (10, 20, 30, 40, and 50 μM), the fluorescence intensity of GSPI continued to decrease, accompanied by a red shift, indicating an interaction between lutein and GSPI, which changed the microenvironment of the fluorophore (53).

Fluorescence quenching includes static quenching, dynamic quenching, and combined static and dynamic quenching. Static quenching is caused by the formation of complexes, whereas dynamic quenching is caused by intermolecular collisions. The dynamic and static combination quenching is caused by the formation of complexes and intermolecular collisions. As shown in **Figure 3B** and **Table 1**, the slope (K_{SV}) of 303 and 313 K was >293 K, indicating that the fluorescence quenching of GSPI was caused by the collision of lutein and GSPI, which was a sign of dynamic quenching. However, the value of K_q

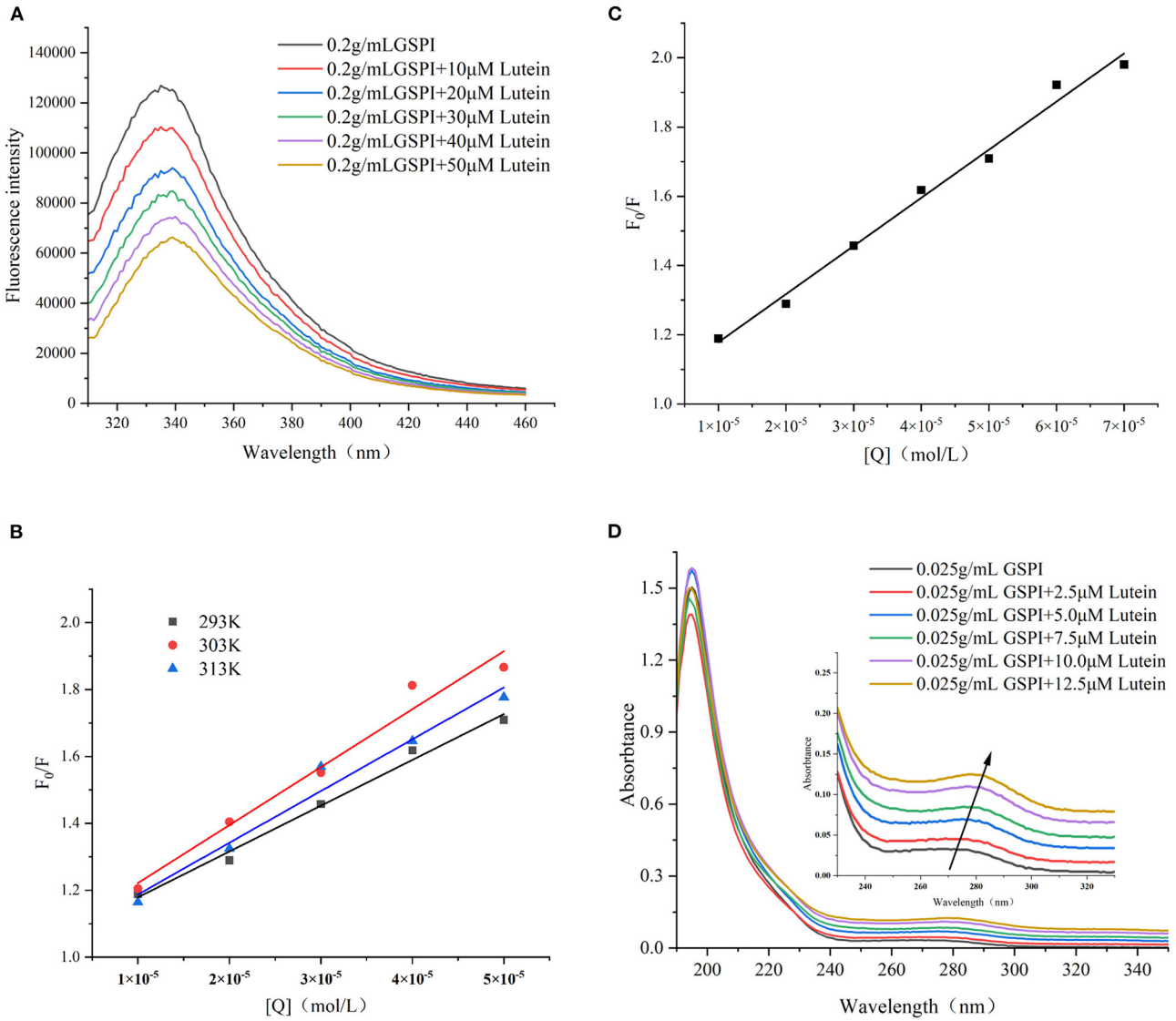

FIGURE 3 | (A) Fluorescence spectra of GSPI (0.2 mg/ml) with different concentrations of lutein (0–50 μM), $T = 293$ K, pH = 7.0, and $\lambda_{ex} = 280$ nm. **(B)** The linear Stern–Volmer plot for lutein binding to GSPI at 293, 303, and 313 K. **(C)** The Stern–Volmer plot for lutein binding to GSPI with lutein (0–70 μM) at 293 K. **(D)** UV–Vis spectra of GSPI (0.2 mg/L) with different concentrations of lutein (0–50 μM), $T = 293$ K, and pH = 7.0.

far exceeded the maximum value of the dynamic quenching rate constant [10^{10}/(mol s)], indicating that the quenching was static. Thus, it could not be concluded if it is a static or dynamic quenching.

The quenching effects of high lutein concentration on GSPI fluorescence and UV–Vis were studied to evaluate the type of quenching between GSPI and lutein. In the case of dynamic quenching, the relationship between F_0/F and high-lutein concentration might concave toward the Y-axis (54). **Figure 3C** depicts a good linear relationship between increasing lutein concentration and F_0/F ($R^2 = 0.9901$), with no concave to the Y-axis (55). It also confirmed that there was no dynamic quenching between lutein and GSPI.

TABLE 1 | Lutein induces the Stern–Volmer quenching constant (K_{SV}) and bimolecular quenching rate (K_q) of GSPI at different temperatures (293, 303, and 313 K).

T (K)	K_{SV} (10^4/mol)	K_q (10^{12}/(mol s))	R^2
293	1.3689	1.3689	0.9899
303	1.7122	1.7122	0.9739
313	1.5495	2.7171	0.9715

Ultraviolet–visible is a simple and effective method for the interaction between small molecules and proteins (56). Dynamic quenching does not change the absorption spectrum of the

fluorophore, whereas complex formation (static quenching) changes the absorption spectrum of the fluorophore (57, 58). As depicted in **Figure 3D**, with the addition of lutein, the absorption intensity of the ultraviolet spectrum increased, which was accompanied by a significant red shift ($\Delta\lambda$ = 10 nm). This indicated that lutein formed a complex with GSPI (59), leading to a red shift in the spectrum (60, 61). Therefore, lutein quenched the fluorescence of GSPI by static quenching.

Binding Forces and Thermodynamic Parameters

The binding constant (K_a value) reflects the strength of the binding force (62). As depicted in **Figure 4**, the lg [$(F_0$-$F)/F$] and lg[Q] presented a good linear relationship ($R^2 > 0.98$). The *n*-values of the three different temperatures at 293, 303, and 313 K were 0.8551, 0.9237, and 0.9861, respectively, indicating that there was only one binding site. The K_a values of lutein and GSPI interaction at 293, 303, and 313 K showed an increasing trend with the increase in temperature (**Table 2**), suggesting that the GSPI–lutein complex was relatively stable at higher temperatures (63).

The thermodynamic parameters, such as ΔG, ΔH, and ΔS, could reveal the GSPI–lutein interaction (64). The value and sign of ΔH and ΔS could reflect the interaction force between small molecules and proteins (65). The forces between the biologically active substances and proteins mainly include hydrophobic interaction, hydrogen bonding, van der Waals force, electrostatic attraction, etc. (66). The interaction force could be divided into four types: for $\Delta H > 0$ and $\Delta S > 0$, the main force is hydrophobic interaction; for $\Delta H > 0$ and $\Delta S < 0$, the main force is electrostatic and hydrophobic interaction; for $\Delta H < 0$ and $\Delta S < 0$, hydrogen bonding and van der Waals force play a major role; and for $\Delta H < 0$ and $\Delta S > 0$, electrostatic interaction plays a principal role (67). As summarized in **Table 2**, $\Delta H > 0$ and $\Delta S > 0$ demonstrated that the interaction force between lutein and GSPI was mainly hydrophobic interaction. Yi et al. (13) reported similar results for WPI and SC (13). Furthermore, the values of ΔG (−20.09, −22.85, and −24.91 kJ mol^{-1}) were negative at 293, 303, and 313 K, indicating spontaneous binding of lutein with GSPI.

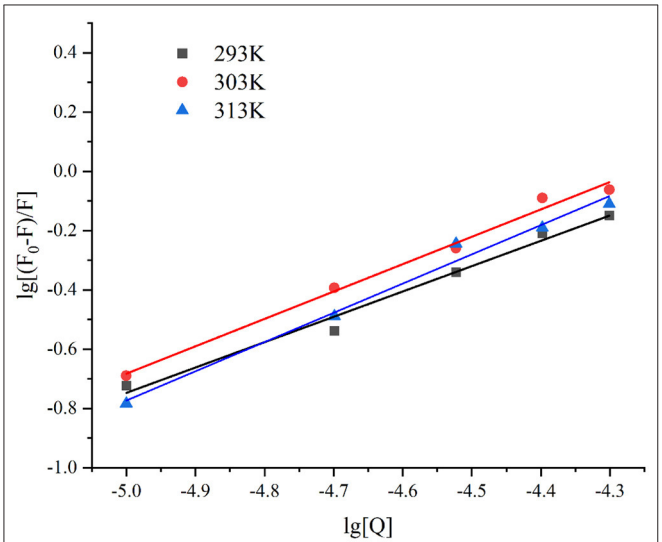

FIGURE 4 | The linear plot of lg [$(F_0$-$F)/F$] against lg [Q] at different temperatures, T = 293, 303, and 313 K.

X-Ray Diffraction

The crystal analysis of the sample was performed by XRD. **Figure 5** depicts the diffraction patterns of lutein, GSPI, and GSPI–lutein. Lutein showed a strong diffraction peak within 10°-25° (2θ), suggesting that lutein had a highly crystalline structure. After the combination of lutein and GSPI, the frontal characteristic diffraction peak of lutein did not appear, showing the presence of lutein in GSPI in an amorphous form (68).

Secondary Structure Analysis

The combined effect of lutein on the structural changes of GSPI was studied by an FTIR. GSPI was used as a control. As described in Section 3.1.2, the amide I region was the most sensitive region related to protein conformation. The amide I region in the FTIR spectra of GSPI and GSPI–lutein was analyzed, and the secondary structural data were obtained by calculating the integrated area of each sub-peak in the 1,600–1,700 cm^{-1} spectrum. The ratio of each secondary structure of GSPI and GSPI–lutein is depicted in **Figure 6**. The FTIR spectra indicated that GSPI–lutein was bound through hydrophobic interaction and had little effect on its secondary structure. These results were consistent with the previous study results reporting that SPIHs interacting with cyanin-3-O-glucoside (Cy3G) (60) and SPI (unheated and heated) combined with curcumin (69) had no significant effect on the secondary structure of the protein.

Effect of GSPI on the Stability of Lutein

Color Analysis

In addition to physiological functions, lutein is also popular as a coloring agent. Therefore, studying its color changes has high significance. The smaller the total color difference (ΔE), the more stable the lutein (70). $\Delta E > 3$ indicated a very significant

TABLE 2 | Binding parameters and thermodynamic parameters of GSPI–lutein system at different temperatures.

T (K)	K_a (10^4 L /mol)	n	R^2	ΔH (kJ mol^{-1})	ΔS (kJ mol^{-1})	ΔG (kJ mol^{-1})
293	0.3189	0.8551	0.9846	50.64	241.79	−20.09
303	0.8701	0.9237	0.9908			−22.85
313	1.4315	0.9861	0.9854			−24.91

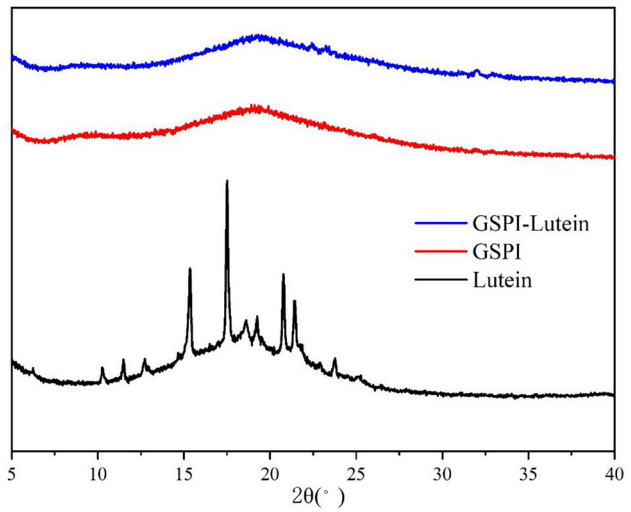

FIGURE 5 | X-ray diffraction of lutein, GSPI, and GSPI–lutein.

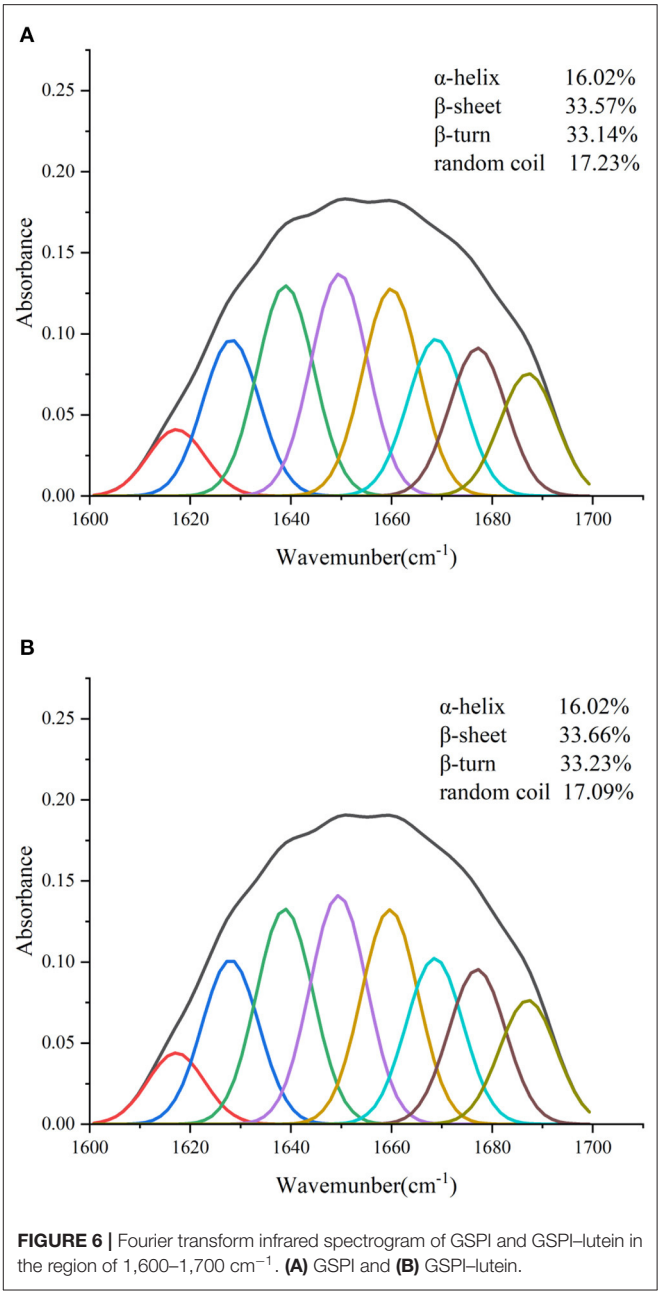

FIGURE 6 | Fourier transform infrared spectrogram of GSPI and GSPI–lutein in the region of 1,600–1,700 cm^{-1}. **(A)** GSPI and **(B)** GSPI–lutein.

difference, $1.5 < \Delta E < 3$ indicated a significant difference, $\Delta E < 1.5$ indicated a small difference (71). As depicted in **Figure 7A**, ΔE of lutein reached 11.83 ± 0.18 at 5 h of light exposure. At this time, the ΔE of SPI–lutein and GSPI–lutein was lower, accounting for 1.04 ± 0.06 and 0.41 ± 0.74, respectively. This result indicated that protein had a positive effect on the photostability of lutein. The difference between SPI–lutein and GSPI–lutein appeared with the prolongation of light time. When the light time was 12 h, the ΔE of SPI–lutein and GSPI–lutein was significantly different, accounting for 7.65 ± 1.34 and 1.91 ± 0.18, respectively. GSPI–lutein exhibited better light stability than lutein and SPI–lutein. However, the advantage of thermal stability was not good as light stability (**Figure 7B**). At 120°C oil bath for 50 min, the ΔE of lutein was 9.42 ± 0.52, the ΔE of SPI–lutein was 6.20 ± 0.08, and the ΔE of GSPI–lutein was 5.58 ± 0.08. Overall, GSPI had a better effect on the color stability of lutein than SPI.

Degradation Rate

Lutein is sensitive to environmental factors, such as light and heat, due to its high degree of unsaturation. **Figure 7C** depicts the degradation rates of lutein, SPI–lutein, and GSPI–lutein under the influence of light and heat, respectively. The degradation rate and total color difference showed the same trend. When lutein was exposed to light for 4 h, the degradation rate reached as high as 95.41% ± 0.34. At this time, the degradation rates of SPI–lutein and GSPI–lutein were 15.78% ± 5.56 and 9.40% ± 2.13, respectively. Compared with lutein, the degradation rate of GSPI–lutein was reduced by about 86.01%. Lutein was completely degraded at 5 h (not shown). With the increase in light time, the degradation rate of GSPI–lutein was always lower than SPI–lutein. Thermal degradation for 10 min showed a significant protective effect of the protein, but there was no significant difference in the protective effect of SPI and GSPI. After 50 min, the degradation rate of lutein was 89.46% ± 0.21, the degradation rate of SPI–lutein was 77.48% ± 0.94, and the degradation rate of GSPI–lutein was 65.96% ± 0.82 (**Figure 7D**). Overall, GSPI–lutein has excellent light stability and fine stability at high temperatures and short time. Additionally, lutein (with or without protein) followed the first-order degradation kinetics at 120°C and zero-order degradation kinetics under UV light at 25°C (**Table 3**).

Particle Size Analysis

The particle size affects the stability of the lutein system (32, 72). The smaller the particle size, the greater the stability in the aqueous solution. As depicted in **Figure 8**, the average particle

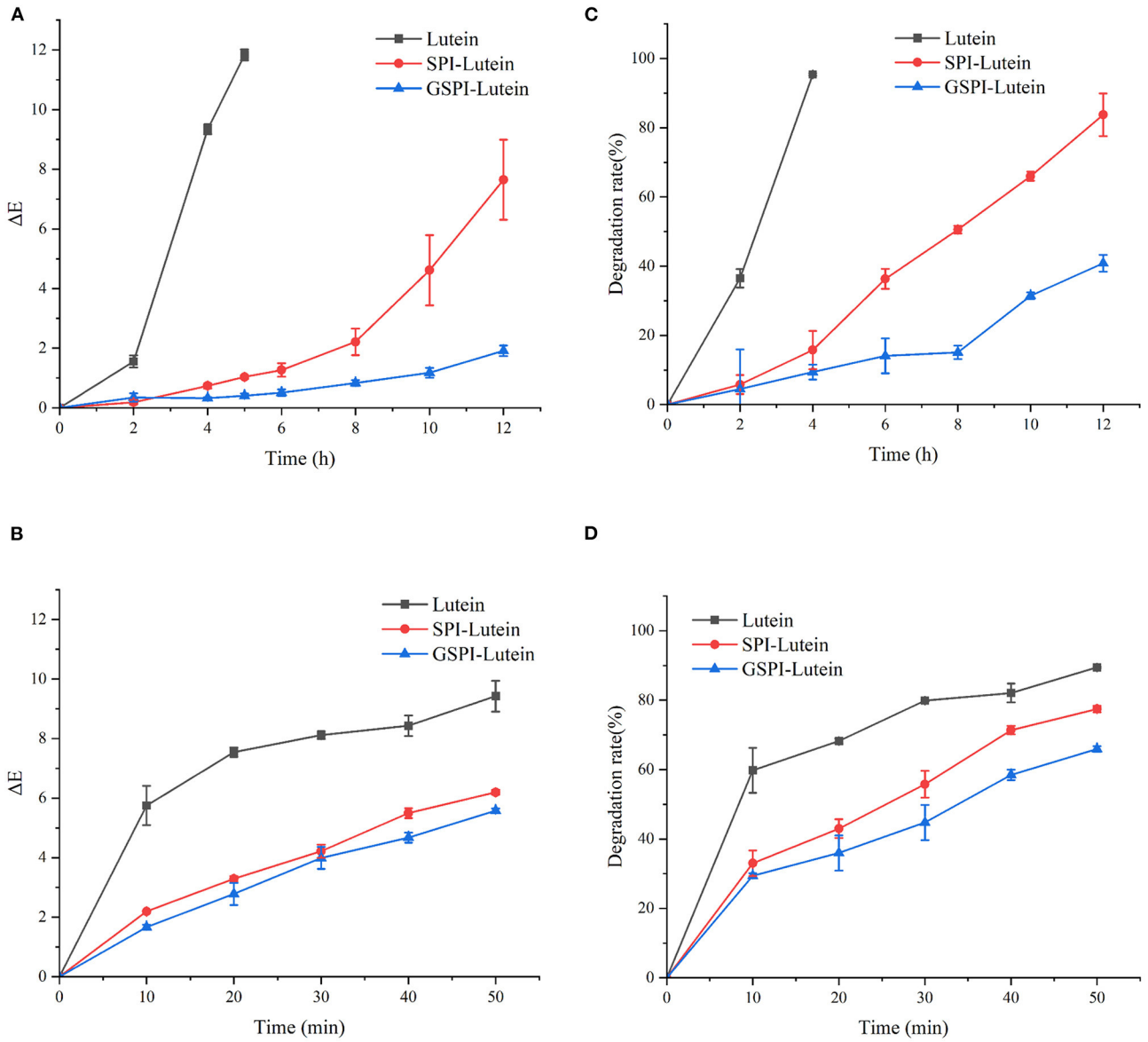

FIGURE 7 | Stability analysis of lutein, SPI–lutein and GSPI–lutein. **(A)** Total color difference under light conditions. **(B)** Total color difference under heating conditions. **(C)** Degradation rate under light conditions. **(D)** Degradation rate under heating conditions.

TABLE 3 | Correlation coefficients of zero-order, first-order, and second-order kinetic models for the lutein degradation.

Correlation coefficient	R_0	R_1	R_2
120°C	0.9676	0.9923	0.9792
25°C UV light	0.9826	0.9677	0.9477

size of lutein in the aqueous solution was about 2 μm. The average particle sizes of SPI and SPI–lutein were about 83.34 and 84.15 μm, respectively. The average particle sizes of GSPI and GSPI–lutein were about 212 and 219 nm, respectively. GSPI and GSPI–lutein had lower particle sizes, indicating that they were more stable in the aqueous solutions.

CONCLUSION

In this study, the effects of glycosylation on the structure and stability of SPI were investigated by fluorescence spectroscopy, FTIR, emulsification, and solubility. The results showed that the glycosylation reaction occurred, and GSPI had better emulsification and solubility than SPI. Then, the interaction between GSPI and lutein was investigated by fluorescence quenching, thermodynamic binding parameters, UV–Vis, and

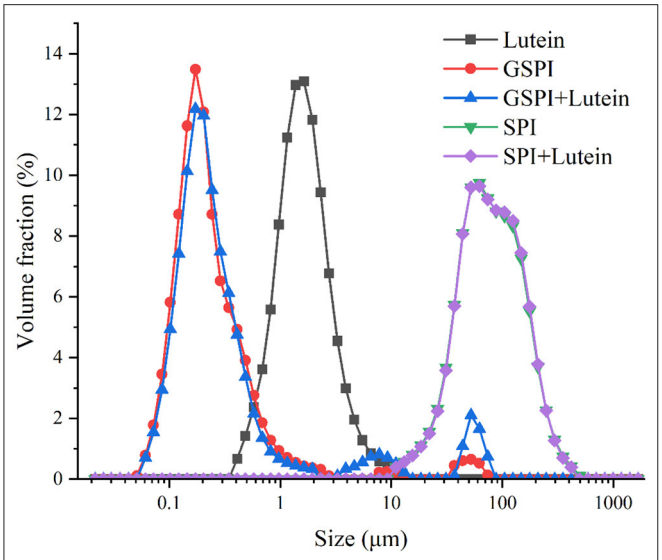

FIGURE 8 | Particle size distribution of lutein, GSPI, GSPI–lutein, SPI, and SPI–lutein.

XRD. The results indicated that lutein was spontaneously bound to GSPI at a stoichiometric of 1:1. The fluorescence of GSPI was quenched by static quenching during the binding process, which slightly affected the secondary structure of GSPI. Finally, the total color difference and degradation rate results showed that GSPI had a better stabilization effect on lutein.

DATA AVAILABILITY STATEMENT

The datasets presented in this study can be found in online repositories. The names of the repository/repositories and accession number(s) can be found in the article/supplementary material.

AUTHOR CONTRIBUTIONS

XW: data management, investigation, validation, and writing—original draft. SW: methodology, project management, and writing—review and editing. DX: fund acquisition and supervision. JP: resources, concepts, and supervision. WG: project management, resources, and capital acquisition. YC: conceptualization, project management, and supervision. All authors contributed to the article and approved the submitted version.

FUNDING

This research was supported by the National Natural Science Foundation of China (31871808), the School Level Cultivation Fund of Beijing Technology and Business University for Distinguished and Excellent Young Scholars (BTBUYP2020), the Construction of Service Capability of Scientific and Technological Innovation (PXM2019_014213_000010, PXM2018_014213_000033, PXM2018_014213_000014, PXM2018_0142 13_000041, and 19005857058), and the Cultivation and Development of Innovation Base (Z171100002217019).

ACKNOWLEDGMENTS

We would like to thank MogoEdit (https://www.mogoedit.com) for its English editing during the preparation of this manuscript.

REFERENCES

1. Chung RWS, Leanderson P, Gustafsson N, Jonasson L. Liberation of lutein from spinach: Effects of heating time, microwavereheating and liquefaction. *Food Chem.* (2019) 277:573–8. doi: 10.1016/j.foodchem.2018.11.023
2. Youjia F, Jingde Y, Longwei J, Lili R, Jiang Z. Encapsulation of lutein into starch nanoparticles to improve its dispersity in water and enhance stability of chemical oxidation. *Starch/Staerke.* (2019) 71:1800248. doi: 10.1002/star.201800248
3. Ziegler JU, Wahl S, Wurschum T, Longin CF, Carle R, Schweiggert RM. Lutein and lutein esters in whole grain flours made from 75 genotypes of 5 triticum species grown at multiple sites. *J Agric Food Chem.* (2015) 63:5061–71. doi: 10.1021/acs.jafc.5b01477
4. Cheng X, Zhao XZ, Huang CL, Zhang XH Lyu YM. Lutein content in petals and leaves of marigold and analysis of lutein synthesis gene expression. *Acta Physiologiae Plantarum.* (2019) 41:128. doi: 10.1007/s11738-019-2913-y
5. Hentschel V, Kranl K, Hollmann J, Lindhauer MG, Bohm V, Bitsch R. Spectrophotometric determination of yellow pigment content and evaluation of carotenoids by high-performance liquid chromatography in durum wheat grain. *J Agric Food Chem.* (2002) 50:6663–8. doi: 10.1021/jf025701p
6. Yoshizako H, Hara K, Takai Y, Kaidzu S, Obana A, Ohira A. Comparison of macular pigment and serum lutein concentration changes between free lutein and lutein esters supplements in Japanese subjects. *Acta Ophthalmol.* (2016) 94:e411–e6. doi: 10.1111/aos.13106
7. Lyu ZJ, Wang F, Liu P, Zhang K, Sun Q, Bai X, et al. One-pot preparation of lutein block methoxy polyethylene glycol copolymer-coated lutein nanoemulsion. *Colloid Polym Sci.* (2021) 299:1055–62. doi: 10.1007/s00396-021-04824-7
8. Rodriguez-Concepcion M, Avalos J, Luisa Bonet M, Boronat A, Gomez-Gomez L, Hornero-Mendez D, et al. A global perspective on carotenoids: Metabolism, biotechnology, and benefits for nutrition and health. *Prog Lipid Res.* (2018) 70:62–93. doi: 10.1016/j.plipres.2018.04.004
9. Horvath MP, George EW, Tran QT, Baumgardner K, Zharov G, Lee S. et al. Structure of the lutein-binding domain of human StARD3 at 174 angstrom resolution and model of a complex with lutein. *Acta Crystallogr F Struct Biol Commun.* (2016) 72:609–18. doi: 10.1107/S2053230X16010694
10. Huang J, Bai F, Wu Y, Ye Q, Liang D, Shi C, et al. Development and evaluation of lutein-loaded alginate microspheres with improved stability and antioxidant. *J Sci Food Agric.* (2019) 99:5195–201. doi: 10.1002/jsfa.9766
11. Steiner BM, McClements DJ, Davidov-Pardo G. Encapsulation systems for lutein: a review. *Trends Food Sci Technol.* (2018) 82:71–81. doi: 10.1016/j.tifs.2018.10.003
12. Qi X, Xu DX, Zhu JJ, Wang SJ, Peng JW, Gao W, et al. Interaction of ovalbumin with lutein dipalmitate and their effects on the color

stability of marigold lutein esters extracts. *Food Chem.* (2022) 372:131211. doi: 10.1016/j.foodchem.2021.131211
13. Yi J, Fan Y, Yokoyama W, Zhang Y, Zhao L. Characterization of milk proteins-lutein complexes and the impact on lutein chemical stability. *Food Chem.* (2016) 200:91–7. doi: 10.1016/j.foodchem.2016.01.035
14. Chee-Yuen G, Wen-Hwei O, Lee-Min W, Azhar Mat E. Effects of ribose, microbial transglutaminase and soy protein isolate on physical properties and in-vitro starch digestibility of yellow noodles. *LWT – Food Sci Technol.* (2009) 42:174–9. doi: 10.1016/j.lwt.2008.05.004
15. Zhang Y, Chen S, Qi B, Sui X, Jiang L. Complexation of thermally-denatured soybean protein isolate with anthocyanins and its effect on the protein structure and in vitro digestibility. *Food Res Int.* (2018) 106:619–25. doi: 10.1016/j.foodres.2018.01.040
16. Sharif HR, Williams PA, Sharif MK, Abbas S, Majeed H, Masamba KG, et al. Current progress in the utilization of native and modified legume proteins as emulsifiers and encapsulants - a review. *Food Hydrocoll.* (2018) 76:2–16. doi: 10.1016/j.foodhyd.2017.01.002
17. Cao JR Li FW, Li YY, Chen HP, Liao XJ, Zhang Y. Hydrophobic interaction driving the binding of soybean protein isolate and chlorophyll: Improvements to the thermal stability of chlorophyll. *Food Hydrocoll.* (2021) 113:106465. doi: 10.1016/j.foodhyd.2020.106465
18. Tapal A, Tiku PK. Complexation of curcumin with soy protein isolate and its implications on solubility and stability of curcumin. *Food Chem.* (2012) 130:960–5. doi: 10.1016/j.foodchem.2011.08.025
19. Wan ZL, Wang JM, Wang LY, Yuan Y, Yang XQ. Complexation of resveratrol with soy protein and its improvement on oxidative stability of corn oil/water emulsions. *Food Chem.* (2014) 161:324–31. doi: 10.1016/j.foodchem.2014.04.028
20. He M. Y., Li L, Wu C, Zheng L, Jiang L, Huang Y, et al. Effects of glycation and acylation on the structural characteristics and physicochemical properties of soy protein isolate. *J Food Sci.* (2021) 86:1737–50. doi: 10.1111/1750-3841.15688
21. Zhang H, Chi Y. Modified soy protein isolate with improved gelling stability by glycosylation under the conditions of ocean shipping. *Int J Food Sci Technol.* (2011) 46:14–22. doi: 10.1111/j.1365-2621.2010.02355.x
22. Zhang Z, Wang X, Yu J, Chen S, Ge H, Jiang L. Freeze-thaw stability of oil-in-water emulsions stabilized by soy protein isolate-dextran conjugates. *Lwt-Food Sci Technol.* (2017) 78:241–9. doi: 10.1016/j.lwt.2016.12.051
23. Jiang L, Li S, Wang N, Zhao S, Chen Y, Chen Y. Preparation of dextran-casein phosphopeptide conjugates, evaluation of its calcium binding capacity and digestion *in vitro*. *Food Chem.* (2021) 352:129332. doi: 10.1016/j.foodchem.2021.129332
24. Liu Y, Zhao GL, Zhao MM, Ren JY, Yang B. Improvement of functional properties of peanut protein isolate by conjugation with dextran through Maillard reaction. *Food Chem.* (2012) 131:901–6. doi: 10.1016/j.foodchem.2011.09.074
25. Wang W, Li C, Bin Z, Huang Q, You L, Chen C, et al. Physicochemical properties and bioactivity of whey protein isolate-inulin conjugates obtained by Maillard reaction. *Int J Biol Macromol.* (2020) 150:326–35. doi: 10.1016/j.ijbiomac.2020.02.086
26. Apolinario AC, Goulart de. Lima Damasceno BP, de Macedo Beltrao NE, Pessoa A, Converti A, da Silva JA. Inulin-type fructans: a review on different aspects of biochemical and pharmaceutical technology. *Carbohydrate Polymers.* (2014) 101:368–78. doi: 10.1016/j.carbpol.2013.09.081
27. Closa-Monasterolo R, Ferre N, Castillejo-DeVillasante G, Luque V, Gispert-Llaurado M, Zaragoza-Jordana M, et al. The use of inulin-type fructans improves stool consistency in constipated children. a randomised clinical trial: pilot study. *Int J Food Sci Nutr.* (2017) 68:587–94. doi: 10.1080/09637486.2016.1263605
28. Coxam V. Current data with inulin-type fructans and calcium, targeting bone health in adults. *J Nutr.* (2007) 137:2527S−33S. doi: 10.1093/jn/137.11.2527S
29. Kleessen B, Blaut M. Modulation of gut mucosal biofilms. *Br J Nutr.* (2005) 93:S35–40. doi: 10.1079/BJN20041346
30. Pool-Zobel BL. Inulin-type fructans and reduction in colon cancer risk: review of experimental and human data. *Br J Nutr.* (2005) 93:S73–90. doi: 10.1079/BJN20041349
31. Roberfroid MB. Introducing inulin-type fructans. *Br J Nutr.* (2005) 93:S13–25. doi: 10.1079/BJN20041350
32. Roberfroid MB. Inulin-type fructans: Functional food ingredients. *J Nutr.* (2007) 137:2493S−502. doi: 10.1093/jn/137.11.2493S
33. Scholz-Ahrens KE, Schrezenmeir J. Inulin and oligofructose and mineral metabolism: The evidence from animal trials. *J Nutr.* (2007) 137:2513S−23. doi: 10.1093/jn/137.11.2513S
34. Boehm A, Kaiser I, Henle T. Heat-induced degradation of inulin. *Eur Food Res Technol.* (2005) 220:466–71. doi: 10.1007/s00217-004-1098-8
35. Qi X, Xu DX, Zhu JJ, Wang SJ, Peng JW, Gao W, et al. Studying the interaction mechanism between bovine serum albumin and lutein dipalmitate: multi-spectroscopic and molecular docking techniques. *Food Hydrocoll.* (2021) 113:106513. doi: 10.1016/j.foodhyd.2020.106513
36. He M, Wu C, Li L, Zheng L, Tian T, Jiang L, et al. Effects of cavitation Jet treatment on the structure and emulsification properties of oxidized Soy Protein Isolate. *Foods.* (2020) 10:2. doi: 10.3390/foods10010002
37. Song JF Li DJ, Pang HL, Liu CQ. Effect of ultrasonic waves on the stability of all-trans lutein and its degradation kinetics. *Ultrason Sonochem.* (2015) 27:602–8. doi: 10.1016/j.ultsonch.2015.04.020
38. Sharafodin H, Soltanizadeh N. Potential application of DBD Plasma Technique for modifying structural and physicochemical properties of Soy Protein Isolate. *Food Hydrocoll.* (2022) 122:107077. doi: 10.1016/j.foodhyd.2021.107077
39. Dursun Capar T, Yalcin H. Protein/polysaccharide conjugation via Maillard reactions in an aqueous media: impact of protein type, reaction time and temperature. *LWT – Food Sci Technol.* (2021) 152:112252. doi: 10.1016/j.lwt.2021.112252
40. Wu Y, Zhang Y, Duan W, Wang Q, An F, Luo P, et al. Ball-milling is an effective pretreatment of glycosylation modified the foaming and gel properties of egg white protein. *J Food Eng.* (2022) 319:110908. doi: 10.1016/j.jfoodeng.2021.110908
41. Zhang Z, Chen W, Zhou X, Deng Q, Dong X, Yang C, et al. Astaxanthin-loaded emulsion gels stabilized by Maillard reaction products of whey protein and flaxseed gum: Physicochemical characterization and in vitro digestibility. *Food Res Int.* (2021) 144:110321. doi: 10.1016/j.foodres.2021.110321
42. Matiacevich SB, Buera MP, A. critical evaluation of fluorescence as a potential marker for the Maillard reaction. *Food Chem.* (2006) 95:423–30. doi: 10.1016/j.foodchem.2005.01.027
43. Hu QH, Wu YL, Zhong L, Ma N, Zhao LY, Ma GX, et al. *In vitro* digestion and cellular antioxidant activity of β-carotene-loaded emulsion stabilized by soy protein isolate-Pleurotus eryngii polysaccharide conjugates. *Food Hydrocoll.* (2021) 112:106340. doi: 10.1016/j.foodhyd.2020.106340
44. Spotti MJ, Martinez MJ, Pilosof AMR, Candioti M, Rubiolo AC, Carrara CR. Influence of Maillard conjugation on structural characteristics and rheological properties of whey protein/dextran systems. *Food Hydrocoll.* (2014) 39:223–30. doi: 10.1016/j.foodhyd.2014.01.014
45. Zhao X, Xing T, Xu X, Zhou G. Influence of extreme alkaline pH induced unfolding and aggregation on PSE-like chicken protein edible film formation. *Food Chem.* (2020) 319:126574. doi: 10.1016/j.foodchem.2020.126574
46. Kang ZL, Bai R, Lu F, Zhang T, Gao ZS, Zhao SM, et al. Effects of high pressure homogenization on the solubility, foaming, and gel properties of soy 11S globulin. *Food Hydrocoll.* (2022) 124:107261. doi: 10.1016/j.foodhyd.2021.107261
47. Xiao H, Huang L, Zhang W, Yin Z. Damage of proteins at the air/water interface: Surface tension characterizes globulin interface stability. *Int J Pharm.* (2020) 584:119445. doi: 10.1016/j.ijpharm.2020.119445
48. Liu Q, Geng R, Zhao J, Chen Q, Kong B. Structural and gel textural properties of Soy Protein Isolate when subjected to extreme acid pH-shifting and mild heating processes. *J Agric Food Chem.* (2015) 63:4853–61. doi: 10.1021/acs.jafc.5b01331
49. Hu YY, Wu Z, Sun YY, Cao JX, He J, Dang YL, et al. Insight into ultrasound-assisted phosphorylation on the structural and emulsifying properties of goose liver protein. *Food Chem.* (2022) 373:131598. doi: 10.1016/j.foodchem.2021.131598
50. Matyus L, Szollosi J, Jenei A. Steady-state fluorescence quenching applications for studying protein structure and dynamics. *J Photochem Photobiol B.* (2006) 83:223–36. doi: 10.1016/j.jphotobiol.2005.12.017
51. Pandit S, Kundu S. Fluorescence quenching and related interactions among globular proteins (BSA and lysozyme) in presence of titanium dioxide

nanoparticles. *Colloids Surfaces a-Physicochem Engineer Aspects.* (2021) 628. doi: 10.1016/j.colsurfa.2021.127253. [Epub ahead of print].
52. Hinderink EBA, Berton-Carabin CC, Schroen K, Riaublanc A, Houinsou-Houssou B, Boire A, et al. Conformational changes of whey and pea proteins upon emulsification approached by front-surface fluorescence. *J Agric Food Chem.* (2021) 69:6601–12. doi: 10.1021/acs.jafc.1c01005
53. Bayraktutan T, Onganer Y. Biophysical influence of coumarin 35 on bovine serum albumin: Spectroscopic study. *Spectrochim Acta A Mol Biomol Spectrosc.* (2017) 171:90–6. doi: 10.1016/j.saa.2016.07.043
54. Wang BL, Pan DQ, Zhou KL, Lou YY, Shi JH. Multi-spectroscopic approaches and molecular simulation research of the intermolecular interaction between the angiotensin-converting enzyme inhibitor (ACE inhibitor) benazepril and bovine serum albumin (BSA). *Spectrochim Acta A Mol Biomol Spectrosc.* (2019) 212:15–24. doi: 10.1016/j.saa.2018.12.040
55. Zhang YF, Zhou KL, Lou YY. Pan Dq, Shi JH. Investigation of the binding interaction between estazolam and bovine serum albumin: multi-spectroscopic methods and molecular docking technique. *J Biomol Struct Dyn.* (2017) 35:3605–14. doi: 10.1080/07391102.2016.1264889
56. You Y, Yang L, Chen H, Xiong L, Yang F. Effects of (–)-Epigallocatechin-3-gallate on the functional and structural properties of Soybean Protein Isolate. *J Agric Food Chem.* (2021) 69:2306–15. doi: 10.1021/acs.jafc.0c07337
57. Zhang D, Zhang X, Liu Y-C, Huang S-C, Ouyang Y, Hu Y-J. Investigations of the molecular interactions between nisoldipine and human serum albumin in vitro using multi-spectroscopy, electrochemistry and docking studies. *J Mol Liq.* (2018) 258:155–62. doi: 10.1016/j.molliq.2018.03.010
58. Tantimongcolwat T, Prachayasittikul S, Prachayasittikul V. Unravelling the interaction mechanism between clioquinol and bovine serum albumin by multi-spectroscopic and molecular docking approaches. *Spectrochim Acta A Mol Biomol Spectrosc.* (2019) 216:25–34. doi: 10.1016/j.saa.2019.03.004
59. Yue Y, Yin C, Huo F, Chao J, Zhang Y. The application of natural drug-curcumin in the detection hypochlorous acid of real sample and its bioimaging. *Sensors Actuators B-Chem.* (2014) 202:551–6. doi: 10.1016/j.snb.2014.05.119
60. Chen Z, Wang C, Gao X, Chen Y, Kumar Santhanam R, Wang C, et al. Interaction characterization of preheated soy protein isolate with cyanidin-3-O-glucoside and their effects on the stability of black soybean seed coat anthocyanins extracts. *Food Chem.* (2019) 271:266–73. doi: 10.1016/j.foodchem.2018.07.170
61. Wang YX, Zhang L, Wang P, Xu XL, Zhou GH. pH-shifting encapsulation of curcumin in egg white protein isolate for improved dispersity, antioxidant capacity and thermal stability. *Food Res Int.* (2020) 137:109366. doi: 10.1016/j.foodres.2020.109366
62. Chen YS, Zhou YF, Chen M, Xie BJ, Yang JF, Chen JG, et al. Isorenieratene interaction with human serum albumin: Multi-spectroscopic analyses and docking simulation. *Food Chem.* (2018) 258:393–9. doi: 10.1016/j.foodchem.2018.02.105
63. Yang L, Baohua L, Lianzhou J, Regenstein JM, Nan J, Poias V, et al. Interaction of soybean protein isolate and phosphatidylcholine in nanoemulsions: a fluorescence analysis. *Food Hydrocoll.* (2019) 87:814–29. doi: 10.1016/j.foodhyd.2018.09.006
64. Lelis CA, Nunes NM, de Paula HMC, Coelho YL, da Silva LHM, Pires ACD. Insights into protein-curcumin interactions: kinetics and thermodynamics of curcumin and lactoferrin binding. *Food Hydrocoll.* (2020) 105:105825. doi: 10.1016/j.foodhyd.2020.105825
65. Mohammadi F, Moeeni M. Study on the interactions of trans-resveratrol and curcumin with bovine alpha-lactalbumin by spectroscopic analysis and molecular docking. *Mater Sci Eng C Mater Biol Appl.* (2015) 50:358–66. doi: 10.1016/j.msec.2015.02.007
66. Song Z, Yuan W, Zhu R, Wang S, Zhang C, Yang B. Study on the interaction between curcumin and CopC by spectroscopic and docking methods. *Int J Macromolecules.* (2017) 96:192–9. doi: 10.1016/j.ijbiomac.2016.11.099
67. Wang C, Xie Y. Interaction of protein isolate with anthocyanin extracted from black Soybean and its effect on the anthocyanin stability. *J Food Sci.* (2019) 84:3140–6. doi: 10.1111/1750-3841.14816
68. Zhao C, Cheng H, Jiang P, Yao Y, Han J. Preparation of lutein-loaded particles for improving solubility and stability by Polyvinylpyrrolidone (PVP) as an emulsion-stabilizer. *Food Chem.* (2014) 156:123–8. doi: 10.1016/j.foodchem.2014.01.086
69. Chen FP Li BS, Tang CH. Nanocomplexation between curcumin and soy protein isolate: influence on curcumin stability/bioaccessibility and in vitro protein digestibility. *J Agric Food Chem.* (2015) 63:3559–69. doi: 10.1021/acs.jafc.5b00448
70. Jimenez-Aguilar DM, Ortega-Regules AE, Lozada-Ramirez JD, Perez-Perez MCI, Vernon-Carter EJ, Welti-Chanes J. Color and chemical stability of spray-dried blueberry extract using mesquite gum as wall material. *J Food Composition Analysis.* (2011) 24:889–94. doi: 10.1016/j.jfca.2011.04.012
71. Bellary AN, Indiramma AR, Prakash M, Baskaran R, Rastogi NK. Anthocyanin infused watermelon rind and its stability during storage. *Innovative Food Sci Emerg Technol.* (2016) 33:554–62. doi: 10.1016/j.ifset.2015.10.010
72. Mengyao L, Fuli W, Chuanfen P, Wenting T, Qingjie S. Nanoencapsulation of lutein within lipid-based delivery systems: characterization and comparison of zein peptide stabilized nano-emulsion, solid lipid nanoparticle, and nano-structured lipid carrier. *Food Chem.* (2021) 358:129840. doi: 10.1016/j.foodchem.2021.129840

Conflict of Interest: JP and WG were employed by Chenguang Biotech Group Co., Ltd.

The remaining authors declare that the research was conducted in the absence of any commercial or financial relationships that could be construed as a potential conflict of interest.

Publisher's Note: All claims expressed in this article are solely those of the authors and do not necessarily represent those of their affiliated organizations, or those of the publisher, the editors and the reviewers. Any product that may be evaluated in this article, or claim that may be made by its manufacturer, is not guaranteed or endorsed by the publisher.